

RESEARCH ARTICLE

Stac proteins associate with the critical domain for excitation–contraction coupling in the II–III loop of Ca_v1.1

 Alexander Polster¹ , Benjamin R. Nelson² , Symeon Papadopoulos³ , Eric N. Olson², and Kurt G. Beam¹ 

In skeletal muscle, residues 720–764/5 within the Ca_v1.1 II–III loop form a critical domain that plays an essential role in transmitting the excitation–contraction (EC) coupling Ca²⁺ release signal to the type 1 ryanodine receptor (RyR1) in the sarcoplasmic reticulum. However, the identities of proteins that interact with the loop and its critical domain and the mechanism by which the II–III loop regulates RyR1 gating remain unknown. Recent work has shown that EC coupling in skeletal muscle of fish and mice depends on the presence of Stac3, an adaptor protein that is highly expressed only in skeletal muscle. Here, by using colocalization as an indicator of molecular interactions, we show that Stac3, as well as Stac1 and Stac2 (predominantly neuronal Stac isoforms), interact with the II–III loop of Ca_v1.1. Further, we find that these Stac proteins promote the functional expression of Ca_v1.1 in tsA201 cells and support EC coupling in Stac3-null myotubes and that Stac3 is the most effective. Coexpression in tsA201 cells reveals that Stac3 interacts only with II–III loop constructs containing the majority of the Ca_v1.1 critical domain residues. By coexpressing Stac3 in dysgenic (Ca_v1.1-null) myotubes together with Ca_v1 constructs whose chimeric II–III loops had previously been tested for functionality, we reveal that the ability of Stac3 to interact with them parallels the ability of these constructs to mediate skeletal type EC coupling. Based on coexpression in tsA201 cells, the interaction of Stac3 with the II–III loop critical domain does not require the presence of the PKC C1 domain in Stac3, but it does require the first of the two SH3 domains. Collectively, our results indicate that activation of RyR1 Ca²⁺ release by Ca_v1.1 depends on Stac3 being bound to critical domain residues in the II–III loop.

Introduction

In skeletal muscle, bidirectional signaling occurs between the dihydropyridine receptor, an L-type Ca²⁺ channel that contains Ca_v1.1 (α_{1S}) as its principle subunit and is located in the plasma membrane, and the type 1 ryanodine receptor (RyR1), which is a Ca²⁺ release channel located in the SR. In response to depolarization of the plasma membrane, Ca_v1.1 transmits an “orthograde” signal that activates RyR1 to release Ca²⁺ (Tanabe et al., 1988; Adams et al., 1990). In addition, a “retrograde” interaction occurs whereby the association with RyR1 increases the magnitude of the voltage-gated Ca²⁺ current carried via Ca_v1.1 (Nakai et al., 1996). The orthograde signal does not require the influx of extracellular Ca²⁺ via the L-type current of Ca_v1.1 (Armstrong et al., 1972), and the retrograde signal does not depend on the Ca²⁺ flux via RyR1 (Avila et al., 2001), which has led to the notion that bidirectional signaling involves conformational coupling between Ca_v1.1 and RyR1.

An approach that has been extensively used in the attempt to identify regions of Ca_v1.1 important for conformational coupling with RyR1 has been to create chimeras between Ca_v1.1, which does support bidirectional signaling, and Ca_v isoforms that do not support such signaling, followed by expression in dysgenic (Ca_v1.1 null) myotubes to assess function. This approach revealed that full bidirectional signaling depends on the presence of a critical domain of ~46 amino acids (residues 720–764/5) within the cytoplasmic II–III loop of Ca_v1.1 (Nakai et al., 1998; Grabner et al., 1999; Wilkens et al., 2001). However, neither the reason why these residues are important for controlling activation of RyR1 nor the identity of proteins they directly contact has been established to date.

One important reason why it has been difficult to elucidate the role of the critical domain in bidirectional signaling between Ca_v1.1 and RyR1 is that this signaling requires the presence of additional proteins. One of these is the β_{1a} auxiliary subunit of

¹Department of Physiology and Biophysics, University of Colorado Denver, Aurora, CO; ²Department of Molecular Biology, Hamon Center for Regenerative Science and Medicine, UT Southwestern Medical Center, Dallas, TX; ³Institute of Vegetative Physiology, University Hospital of Cologne, Cologne, Germany.

Correspondence to Kurt Beam: kurt.beam@ucdenver.edu.

© 2018 Polster et al. This article is distributed under the terms of an Attribution–Noncommercial–Share Alike–No Mirror Sites license for the first six months after the publication date (see <http://www.rupress.org/terms/>). After six months it is available under a Creative Commons License (Attribution–Noncommercial–Share Alike 4.0 International license, as described at <https://creativecommons.org/licenses/by-nc-sa/4.0/>).

Ca_v1.1. As for other Ca_vβ and high-voltage-activated Ca²⁺ channel isoforms, β_{1a} facilitates membrane trafficking of Ca_v1.1 (Beurg et al., 1999; Schredelseker et al., 2009). Additionally, the ability of Ca_v1.1 to transmit the orthograde excitation-contraction (EC) coupling signal to RyR1 depends on the presence of specific sequences within β_{1a} (Beurg et al., 1999; Schredelseker et al., 2009). A second, recently discovered protein of similar importance is Stac3, one of three isoforms of Stac protein; Stac3 is highly expressed in skeletal muscle, whereas Stac1 and Stac2 are predominantly expressed in nervous tissue (Nelson et al., 2013). Membrane expression is reduced (Polster et al., 2016) and EC coupling ablated in mouse and fish muscle null for Stac3 (Horstick et al., 2013; Nelson et al., 2013). Membrane expression, but not EC coupling, is largely restored in mouse muscle (Polster et al., 2016) by a Stac3 construct bearing a point mutation that is responsible for a severe, recessively inherited myopathy (Horstick et al., 2013). Thus, Stac3 appears to play a crucial role in EC coupling, but just as for the critical domain of Ca_v1.1, the molecular interactions underlying this role have not been elucidated.

Our previous work indicated that Stac3 binds directly to Ca_v1.1 (Polster et al., 2015) but did not identify the regions of both proteins responsible for their binding to one another. All three Stac isoforms contain a PKC C1 domain and SH3 domains, although sequence of each of these domains varies somewhat between isoforms. The regions linking these conserved domains vary between isoforms. Campiglio and Flucher (2017) analyzed the ability of Stac protein constructs to cluster at plasma membrane-SR junctions in dysgenic myotubes. Specifically, they compared clustering abilities of Stac3 with those of Stac1 and Stac2, as well as the clustering abilities of Stac3/Stac2 chimeras and Stac3 bearing one or more amino acid substitutions. They concluded that the PKC C1 domain of Stac3 is important for its binding to Ca_v1.1.

Here, we used a different set of approaches. One of these was to compare the abilities of Stac1, Stac2, and Stac3 to support membrane expression of Ca_v1.1 in tsA201 cells and restore EC coupling in Stac3-null myotubes. Another was to assess interactions between the fluorescently tagged Stac proteins and Ca_v constructs after their coexpression in tsA201 cells, because interactions observed in these cells are likely to be directly between the expressed proteins. We used both the full-length Ca_v constructs that had been previously tested for function in dysgenic myotubes and isolated Ca_v1.1 cytoplasmic domains coupled to a sequence (the I-II loop of Ca_v1.2) that had been shown to traffic to the surface membrane of tsA201 cells (Takahashi et al., 2005; Kaur et al., 2015). Based on colocalization as an indicator of interaction, we concluded that all three Stac isoforms bound to the Ca_v1.1 II-III loop. All three isoforms also interacted, to varying extents, with Ca_v1.1 in tsA201 cells and Stac3-null myotubes. Moreover, subdivision of the II-III loop indicated that the domain previously shown to be functionally critical for bidirectional signaling (residues 720-764/5) was also important for the binding of Stac3. As another approach, we expressed fluorescently tagged Stac proteins in dysgenic myotubes together with fluorescently tagged, full-length Ca_v constructs. This approach revealed that, as in tsA201 cells, Stac3 binding in muscle cells depended on sequence contained within the critical domain of the II-III loop.

Thus, our results on Stac3 interactions suggest a previously unknown role for the critical domain, which is that it is required for the binding of Stac3, which in turn is required for the ability of Ca_v1.1 to transmit the EC coupling signal to RyR1.

Materials and methods

Molecular biology

The construction of the expression plasmids for GFP-Ca_v1.1, YFP-Ca_v1.1, GFP-SkLC, GFP-SkLCS₄₆, GFP-SkLCS₁₈, GFP-SkLM, GFP-SkLMS₄₅, unlabeled β_{1a}, Stac2-YFP, Stac3-YFP, unlabeled Stac2, and unlabeled Stac3 was described previously (Grabner et al., 1998, 1999; Wilkens et al., 2001; Papadopoulos et al., 2004; Polster et al., 2015). The expression vectors for YFP-Ca_v1.1 (Papadopoulos et al., 2004) and YFP-Ca_v1.2 (Polster et al., 2015) were used as templates to amplify the sequence of defined, cytoplasmic domains of the channels via standard PCR. Subsequent digestion of the PCR products at restriction sites introduced at both ends during amplification allowed for later ligation into the multiple cloning site of pEGFP-C1 (Clontech). The following is a list of the constructs used in this study, of their forward (fw) and reverse (rev) primers with the respective enzymes used for restriction, followed by the range of encoded rabbit Ca_v1.1 (GenBank: X05921.1), Ca_v1.2 (GenBank: X15539.1), and *Musca domestica* Ca_v1.1 (Wilkens et al., 2001) amino acid residues: GFP-N-term(Ca_v1.1): fw 5'-GAACCGTCATGGAGCCATCTCA CCCCAG-3', AgeI, rev 5'-GTACCGTTTCCATTCCACGATGCTGATG-3', AgeI, residues 1-52; GFP-I-II(Ca_v1.1): fw 5'-GGGGTACCG GGAATTCACCAAGGAGCG-3', KpnI, rev 5'-CCCCGGGCTCG ACTTACCAGGTCATGGC-3', XmaI, residues 335-431; GFP-II-III(Ca_v1.1): fw 5'-GATTGTGACAACCTGGCCGAGGCGGAG-3', SalI, rev 5'-GTGGATCCAGGTGGCGTTGACGATGCGG-3', BamHI, residues 660-800; GFP-662-730(Ca_v1.1): fw 5'-GCAGTCGAC AACCTGGCCGAGGCGGAGAGC-3', SalI, rev 5'-GGCGGATCCCTA GTTGACGTTAGATTCCAAC-3', BamHI, residues 662-730; GFP-697-765(Ca_v1.1): fw 5'-GCAGTCGACGAGAAGTCTGTGATGGCC AAG-3', SalI, rev 5'-GGCGGATCCCTACTGCAGCTCGGCCAGCGG GC-3', BamHI, residues 697-765; GFP-731-799(Ca_v1.1): fw 5'-GCA GTCGACGAGGTGAAGGACCCCTACCCTTC-3', SalI, rev 5'-GGC GGATCCCTAGGTGGCGTTGACGATGCGG-3', BamHI, residues 731-799; GFP-III-IV(Ca_v1.1): fw 5'-CAGGTACCGTCACCTTCCAGG AGCAG-3', KpnI, rev 5'-GTCCCGGGAGGAGGTGACGACGTACC-3', XmaI, residues 1,066-1,118; GFP-C-term(Ca_v1.1): fw 5'-GCAGTC GACTTTGACTACCTGACACGCGAC-3', SalI, rev 5'-GGCGGTACC CTACTGGTCAAGGCTGCCAGG-3', KpnI, residues 1,384-1,855; GFP-I-II(Ca_v1.2): fw 5'-GCAGTCGACGAGAGTTTTCCAAAGAG AGG-3', SalI, rev 5'-GGCGGATCCCTAGTTGACTTGACCGCTGCG-3', BamHI, residues 436-554; GFP-II-III(Ca_v1.2), GFP-II-III(SkLCS₄₆), GFP-II-III(SkLCS₁₈): fw 5'-GCAGTCGACAACCTGGCT GATGCTGAGAGC-3', SalI, rev 5'-GGCGGATCCCTACGTGTCGTT GACGATACGG-3', BamHI, residues 784-930; GFP-II-III(SkLM), GFP-II-III(SkLMS₄₅): fw 5'-GCAGTCGACGATAACTTAGCAGAC GCTG-3', SalI, rev 5'-GGCGGATCCCTAGGTGGCGTTGACGAT GCGG-3', BamHI, residues 665-790.

To add the Ca_v1.2 I-II-loop sequence to these GFP-labeled intracellular Ca_v domains, PCR with the primers fw 5'-GCCTCG AGGAGAGTTTTCCAAAGAGAGG-3' and rev 5'-GCAAGCTTCCTT

GACCGCTGCGGGCACTTTC-3' was used to introduce XhoI and HindIII sites flanking the I-II loop (residues 436–552) of Ca_v1.2 from which the I-II loop-containing XhoI–HindIII fragment was inserted into the plasmids of GFP-labeled cytoplasmic domains of Ca_v1.1 and the II–III loops of SkLC, SkLCS₄₆, SkLCS₁₈, SkLM, or SkLMS₄₅.

PCR with the primers fw 5'-CTGAGGTACCAACCATGATTCCTCCAAGTGGGCGC-3' and rev 5'-GTGGTACCAACACGTCTACCA GTACATCC-3' or rev 5'-GTGGTACCTACACGTCTACCAGTACATCC-3' was used to introduce KpnI sites, or KpnI sites and a stop codon, flanking the coding sequence for Stac1 (gene ID 20840; Cedarlane Laboratories), from which the KpnI–KpnI fragments were inserted into EYFP-N1 (Clontech) to create Stac1-YFP or into pECFP-N1 (Clontech). Afterward, the latter construct was digested with NdeI and BamHI, and the fragment containing the Stac1 sequence was then ligated to the 3,575-bp fragment of pEYFP-C1 (Clontech) that had been digested with the same enzymes to produce the expression vector for unlabeled Stac1.

PCR with the primers fw 5'-GCTGGTTTAGTGAACCGTCAGATCCGCTAGC-3' and rev 5'-GTGCGGCCGCTAATTAAGTTTGTGCCCCAGTTTGC-3' was used to amplify the coding sequence for tagRFP from tagRFP-C1 (Clontech) and to introduce AgeI and NotI sites flanking tagRFP and a stop codon. The AgeI–NotI fragment was then inserted into the vector encoding for EYFP-N1 (Clontech) to create tagRFP-N1. To create Stac3-RFP, the tagRFP-containing fragments from tagRFP-N1 was inserted into Stac3-YFP (Polster et al., 2015), using the restriction enzymes BamHI and NotI. To create Stac1- or Stac2-RFP, the Stac1- or Stac2-containing fragments from Stac1-YFP or Stac2-YFP (Polster et al., 2015) replaced Stac3 in Stac3-RFP, using the restriction enzymes NdeI and BamHI.

PCR with the fw primer 5'-GCAGAATTCATGCACAAGTTCAAA GATCAC-3', 5'-GCAGAATTCATGTTCCGTCGGGCCTATAGC-3', or 5'-GCAGAATTCATGGGAGAACGTGTGCACCGC-3' and rev primer 5'-GGCGGATCCGCAATCTCCTCCAGGAAGTCG-3' was used to introduce EcoRI and BamHI sites flanking the coding sequence for Stac3 fragments from which the EcoRI–BamHI fragment was inserted into tagRFP-N1 to create Stac3(Δ87)-RFP, Stac3(Δ146)-RFP, and Stac3(Δ302)-RFP, respectively. To produce unlabeled Stac3(Δ146) for electrophysiological experiments, PCR with the primers fw 5'-GCAGAATTCATGTTCCGTCGGGCCTATAGC-3' and rev 5'-GTGGTACCTAAATCTCCTCCAGGAAGTCG-3' was used to introduce EcoRI and KpnI sites and a stop codon flanking the coding sequence for Stac3, from which the EcoRI–KpnI fragment was inserted into the vector of unlabeled Stac1 (see above) that had been digested with the same enzymes.

The α₂-δ₁ subunit was kindly provided by William A. Sather (University of Colorado, Denver, CO). All constructs were verified by enzyme digestion and sequence analysis.

tsA201 cell culture and expression of cDNA

tsA201 cells were propagated in high-glucose DMEM supplemented with 10% (vol/vol) FBS and 2 mM glutamine in a humidified incubator with 5% (vol/vol) CO₂. Cells were plated at a density of 2 × 10⁵ cells in 35-mm dishes and transfected 24 h later with jetPRIME (Polyplus-transfection Inc.) with various cDNA combinations of GFP-Ca_v1.1, YFP-Ca_v1.1 (1 μg/dish), β_{1a}, α₂-δ₁, GFP

(and Ca_v1.2 I–II loop)-labeled intracellular channel regions, and unlabeled or RFP-labeled Stac protein isoforms or fragments (0.5 μg/dish). 4 h after transfection, cells were removed from the dish, using Trypsin EDTA (Mediatech), split 1:2 into fresh medium, and replated into 35-mm culture dishes with glass-coverslip bottoms (MatTek) for imaging or at ~1 × 10⁴ cells per 35-mm culture dish to obtain isolated cells for electrophysiological recording. Approximately 48 h after transfection, positively transfected cells were identified by the pattern of yellow or green (and red) fluorescence and were used for electrophysiology or imaging.

Primary skeletal muscle cell culture and cDNA microinjection

All procedures involving mice were approved by the University of Colorado Denver-Anschutz Medical Campus Institutional Animal Care and Use Committee. Myoblasts from newborn dysgenic mice homozygous for absence of Ca_v1.1 (a total of four independent culture preparations; Tanabe et al., 1988) or embryonic day 18.5 fetuses, homozygous or heterozygous for the absence of Stac3 (a total of two independent culture preparations each), were prepared as described before (Beam and Franzini-Armstrong, 1997; Nelson et al., 2013). Myoblasts were plated into 35-mm culture dishes with ECL-coated glass-coverslip bottoms. Cultures were grown in a humidified 37°C incubator with 5% (vol/vol) CO₂ in high-glucose DMEM (Mediatech) supplemented with 10% (vol/vol) FBS and 10% (vol/vol) horse serum (both from HyClone Laboratories). After 4–5 d, this medium was replaced with differentiation medium (DMEM supplemented with 2% [vol/vol] horse serum). 2–4 d after the shift to differentiation medium, single nuclei were microinjected with plasmid cDNA (150 ng/μl for GFP-labeled full-length channels, 20 ng/μl for Stac constructs, and/or 5 ng/μl for BFP [pmTagBFP2-N1; Addgene] in water). 48 h after injection, expressing cells were identified on the basis of GFP and tagRFP, BFP, or YFP fluorescence.

Confocal microscopy, photobleaching, and colocalization quantification

Myotubes or tsA201 cells were superfused with rodent Ringer's solution (146 mM NaCl, 5 mM KCl, 2 mM CaCl₂, 1 mM MgCl₂, and 10 mM HEPES, pH 7.4, with NaOH) and examined using a Zeiss LSM 710 confocal microscope. Excitation and emission (nanometers) for the fluorescent proteins were GFP (ex: 488, em: 493–590), YFP (ex: 514, em: 530–565), and tagRFP (ex: 543, em: 582–754). Relative to full power output, the excitation was attenuated to ~1% (488 nm), ~2% (514 nm), and ~2–4% (543 nm). Images were obtained with a 40× (1.3 numerical aperture) oil-immersion objective as a single, midlevel optical slice that was halfway between the substrate and upper cell surface for tsA201 cells and near the substrate for myotubes. For comparing the distribution of labeled Stac and Ca_v constructs, myotubes were selected on the basis of a punctate distribution of the labeled Ca_v construct. tsA201 cells were selected for subsequent analysis on the basis of isolation from surrounding cells and an initial mid-level optical scan displaying (1) close association of the tagged Ca_v construct with the perimeter of the cell and (2) high expression of the tagged Stac construct as judged by a uniformly strong fluorescence throughout the entire optical section. The mobile fraction of the tagged Stac was then photobleached by repeatedly scanning for 15–45 s

with nonattenuated excitation within a region of interest that was designated to avoid the cell surface. A second midlevel scan acquired afterward was used to assess colocalization.

To quantify colocalization, the fluorescence intensity of Stac-RFP fluorescence was compared with that of GFP-labeled Ca_v constructs ZEN 2.3 SP1 (Black) software (Carl Zeiss Microscopy). After subtraction of background intensity measured in a cell-free region, a digital mask (compare Fig. 6 of Papadopoulos et al., 2004) was produced by application of an adjustable threshold to the GFP image such that all pixel values at or below the threshold were excluded from analysis, and all values above the threshold (i.e., the majority of the surface-associated fluorescence in tsA201 cells or the fluorescent puncta in myotubes) were included. For those Ca_v constructs that produced aggregates in the interior of tsA201 cells (see Fig. 4), the mask was created only from the regions of the cell in which the interior aggregates were absent. Pearson's coefficients for colocalization of green and red fluorescence within the digital mask were calculated as

$$\text{PCC} = \frac{\sum_{i=1}^n (F_{EGFP,i} - \overline{F_{EGFP}}) \cdot (F_{RFP,i} - \overline{F_{RFP}})}{\sqrt{\sum_{i=1}^n (F_{EGFP,i} - \overline{F_{EGFP}})^2 \cdot \sum_{i=1}^n (F_{RFP,i} - \overline{F_{RFP}})^2}} \quad (1)$$

where $F_{EGFP,i}$ and $F_{RFP,i}$ are the background-corrected fluorescence intensities (F) measured for EGFP-labeled channel (fragments) with tagRFP-labeled Stac constructs at the i^{th} pixel, respectively. n is the total pixel number of the generated mask, and $\overline{F_{EGFP}}$ and $\overline{F_{RFP}}$ are the mean F values for that mask.

To measure the dissociation of Stac3 from $\text{Ca}_v1.1$, dysgenic myotubes injected with cDNAs for GFP- $\text{Ca}_v1.1$ and Stac3-RFP were washed 48 h after injection with "internal solution" consisting of (mM) 140 Cs-aspartate, 10 Cs₂-EGTA, 5 MgCl₂, and 10 HEPES, pH 7.4, with CsOH. The myotubes were then permeabilized with saponin (12 $\mu\text{g}/\text{ml}$ in internal solution) for 30 s, washed twice with internal solution, and thereafter imaged immediately (0 min) and 5, 15, 30, 45, and 60 min later. The ratio of red to green fluorescence intensity (I_R/I_G) was calculated at these time points after creation of a digital mask as described above.

Measurement of L-type Ca^{2+} currents

All experiments were performed at room temperature ($\sim 25^\circ\text{C}$). Pipettes ($\sim 2.0 \text{ M}\Omega$) were filled with internal solution (see above). The external solution contained (in millimolar) 145 tetraethylammonium-Cl, 10 CaCl_2 , and 10 HEPES, pH 7.4, with tetraethylammonium-OH. L-type currents were measured in response to test pulses applied directly from the holding potential (-80 mV). Electronic compensation was used to reduce the effective series resistance to $< 5 \text{ M}\Omega$ (time constant $< 400 \mu\text{s}$). Linear components of leak and capacitive current were corrected with $-P/4$ online subtraction protocols. Filtering was at 2–5 kHz and digitization was at 10 kHz. Cell capacitance was determined by integration of a transient elicited by stepping from the holding potential to -70 mV using Clampex 8.2 (Molecular Devices) and was used to normalize ionic currents (picoamperes per picofarad). Peak I–V curves were fitted according to:

$$I = G_{\text{max}}(V - V_{\text{rev}}) / \{1 + \exp[-(V - V_{1/2})/k_G]\}, \quad (2)$$

where I is the peak current for the test potential V , V_{rev} is the reversal potential, G_{max} is the maximum Ca^{2+} channel conductance, $V_{1/2}$ is the half-maximal activation potential and k_G is the slope factor.

Measurement of intracellular Ca^{2+} transients

Changes in intracellular Ca^{2+} were recorded with Fluo-3 (Molecular Probes) in the whole-cell patch-clamp configuration (see above). The salt form of the dye was added to the standard internal solution for a final concentration of 200 nM. After entry into the whole-cell configuration, a waiting period of $> 5 \text{ min}$ was used to allow the dye to diffuse into the cell interior. A Zeiss LSM 710 was used to excite the dye (488 nm) and measure fluorescence emission (519–585 nm) in the voltage-clamped myotube during 200-ms test pulses. Fluorescence data are expressed as $\Delta F/F$, where ΔF represents the peak change in fluorescence from baseline during the test pulse and F is the fluorescence immediately before the test pulse minus the mean background (non-Fluo-3) fluorescence. The fluorescence change ($\Delta F/F$) for each test potential (V) was fitted according to

$$(\Delta F/F) = (\Delta F/F)_{\text{max}} / \{1 + \exp[(V_F - V)/k_F]\}, \quad (3)$$

where $(\Delta F/F)_{\text{max}}$ is the maximal fluorescence change, V_F is the potential causing half the maximal change in fluorescence, and k_F is a slope parameter.

Analysis

The software program SigmaPlot (version 11.0; SSPS) was used for statistical analysis, curve fitting, and preparation of figures. All data are presented as mean \pm SEM.

Online supplemental material

Fig. S1 shows Stac proteins do not associate intrinsically with the surface of tsA201 cells. Fig. S2 shows Stac proteins do not interact with the GFP-tagged I–II loop of $\text{Ca}_v1.2$. Fig. S3 shows Stac1 associates specifically with the $\text{Ca}_v1.1$ II–III loop in tsA201 cells. Fig. S4 shows Stac2 associates specifically with the $\text{Ca}_v1.1$ II–III loop in tsA201 cells.

Results

Our initial strategy in this work was to determine whether differences between the predominantly neuronal Stac isoforms (Stac1 and Stac2) and the muscle isoform (Stac3) could be exploited as a means of identifying domains of Stac3 important for its interactions with $\text{Ca}_v1.1$. Previously, we had found that Ca^{2+} currents were absent in tsA201 cells transfected only with $\text{Ca}_v1.1$, β_{1a} and $\alpha_2\text{-}\delta_1$. However, in cells transfected with $\text{Ca}_v1.1$, β_{1a} and $\alpha_2\text{-}\delta_1$ plus Stac3, Stac3, and $\text{Ca}_v1.1$ were colocalized at the cell surface and robust Ca^{2+} currents were present (Polster et al., 2015). Here, we tested the extent to which Stac1 and Stac2 could substitute for Stac3 in tsA201 cells (Fig. 1). To assess association at the surface, we used fluorescently tagged constructs of $\text{Ca}_v1.1$ and Stac and applied strong illumination within the cellular interior to selectively bleach the mobile fraction of the labeled Stac construct. As shown

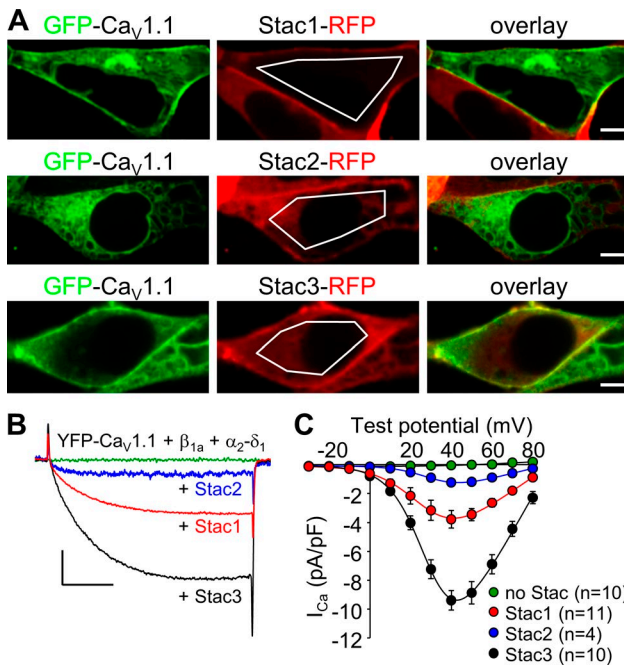


Figure 1. All three Stac isoforms interact with full-length $Ca_v1.1$ and promote its functional expression in tsA201 cells. (A) Representative images of tsA201 cells cotransfected with GFP- $Ca_v1.1$, β_{1a} , $\alpha_2\text{-}\delta_1$, and either Stac1-RFP (top), Stac2-RFP (middle), or Stac3-RFP (bottom). Here, and in subsequent figures, images were obtained after red fluorescence was bleached within the indicated regions of interest. Bars, 5 μm . (B and C) Comparison of representative peak Ca^{2+} currents (B; $V_{\text{test}} = +40$ mV) and mean peak I-V relationships (C; mean \pm SEM) in tsA201 cells cotransfected with YFP- $Ca_v1.1$, β_{1a} and $\alpha_2\text{-}\delta_1$ either without Stac (green) or with Stac1 (red), Stac2 (blue), or Stac3 (black). Calibrations: 3 pA/pF (vertical), 50 ms (horizontal). The Ca^{2+} currents in B and peak I-V relationships in C obtained with Stac3, or without any Stac protein, are replotted from Polster et al. (2015).

previously for Stac3 (Polster et al., 2015), no surface associated fluorescence was observed after application of this procedure to cells transfected only with labeled Stac1 or Stac2 (Fig. S1). However, fluorescently tagged Stac1 and Stac2 both remained associated with the surface when $Ca_v1.1$ was also present (Fig. 1 A). Additionally, both Stac1 and Stac2 were able to support functional expression of $Ca_v1.1$, although to a lesser extent than Stac3 (Fig. 1, B and C). Stac1 and Stac2 also appeared to function as partial substitutes for Stac3 in muscle cells null for endogenous Stac3. Thus, Stac1 and Stac2 displayed a punctate distribution when expressed in Stac3-null myotubes, which was similar to that of Stac3 (Fig. 2 A) and is consistent with binding to $Ca_v1.1$ at plasma membrane junctions with the SR (Polster et al., 2015). Moreover, Stac1 and Stac2 restored depolarization-evoked Ca^{2+} release in Stac-null myotubes to a level $\sim 40\%$ of that restored by expression of Stac3 (Fig. 2 B).

Based on the results above, we next investigated whether the three Stac isoforms differed in their binding to one or more of the cytoplasmic domains of $Ca_v1.1$ (illustrated schematically in Fig. 3 A, dashed box). Expressed in tsA201 cells, the $Ca_v1.1$ II-III loop accumulated in bands around the nucleus, whereas the other cytoplasmic domains were diffusely present in the cytoplasm and, to some extent, diffusely distributed within the nucleus and also in small aggregates (Fig. 3 A). In the case of the I-II loop, a weak association with the surface could be observed

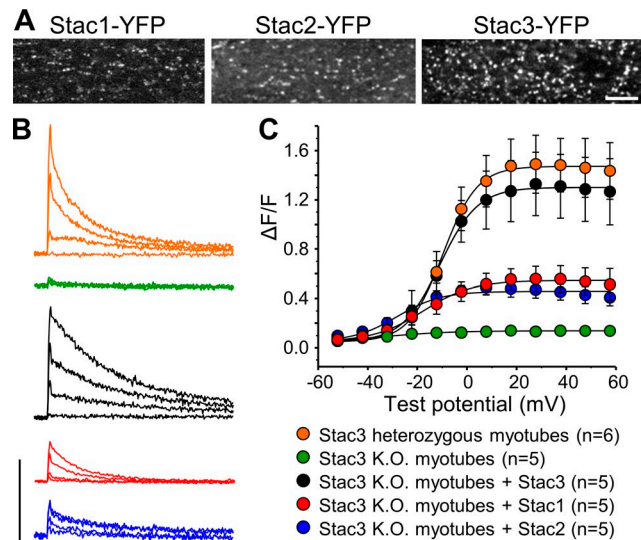


Figure 2. Expression of Stac1 or Stac2 in Stac3-null myotubes restores EC coupling Ca^{2+} release, although to a lesser extent than Stac3. (A) Confocal scans near the surface reveal that after expression in Stac3-null myotubes, Stac1-YFP (left), Stac2-YFP (middle), and Stac3-YFP (right) were similarly distributed in a punctate fashion, consistent with targeting to plasma membrane junctions with the SR. Bar, 5 μm . (B and C) Representative Ca^{2+} transients measured with Fluo-3 (B) and peak fluorescence change (C; $\Delta F/F$, mean \pm SEM) as a function of test potential for myotubes from mice heterozygous for Stac3 KO (orange), null for Stac3 (green), or null for Stac3 and transfected with Stac3 (black), Stac1 (red), or Stac2 (blue). Test depolarizations were 200 ms in duration and applied from a -80 mV holding potential. In B, test potentials were -40 , -20 , 0 , and $+20$ mV and the calibrations represent 1 $\Delta F/F$ (vertical) and 5 s (horizontal). The Stac constructs were unlabeled, and transfected cells were identified on the basis of cotransfected blue fluorescent protein (BFP). The Ca^{2+} transients and $\Delta F/F$ data for myotubes from mice heterozygous or homozygous for Stac3 KO, and for Stac3 KO myotubes transfected with Stac3, are replotted from Polster et al. (2016).

after extensive bleaching of the mobile fraction within the cell interior (not depicted). However, to obtain a subcellular distribution more favorable for comparing interactions with Stac proteins, we linked the $Ca_v1.1$ cytoplasmic domains to the I-II loop of $Ca_v1.2$, which had been shown to provide a higher signal to noise ratio (surface vs. interior) in tsA201 cells (Kaur et al., 2015). As expected, we found that the GFP-tagged $Ca_v1.2$ I-II loop strongly associated with the cell surface (Fig. 3 B, dashed box), and this was also the case after its linkage to the $Ca_v1.1$ cytoplasmic domains (Fig. 3 B). Thus, fusions to the targeting sequence (GFP-tagged $Ca_v1.2$ I-II loop) were used for all subsequent experiments on Ca_v cytoplasmic domains in tsA201 cells. In control experiments, comparison of pre and postbleach images (Fig. S2) demonstrated that none of the three Stac isoforms bound to the surface-targeting construct, GFP-I-II($Ca_v1.2$).

Fig. 4 illustrates images of cells coexpressing Stac3-RFP and $Ca_v1.1$ cytoplasmic domains (fused to the surface-targeting sequence), obtained after bleaching of RFP within the indicated regions of interest (ROI) in the cell interior. Of the five cytoplasmic domains, Stac3-RFP showed a clear association only with the II-III loop. Similarly, the II-III loop was the only cytoplasmic domain with which Stac1 (Fig. S3) and Stac2 (Fig. S4) showed a clear association. The preferential association between each of

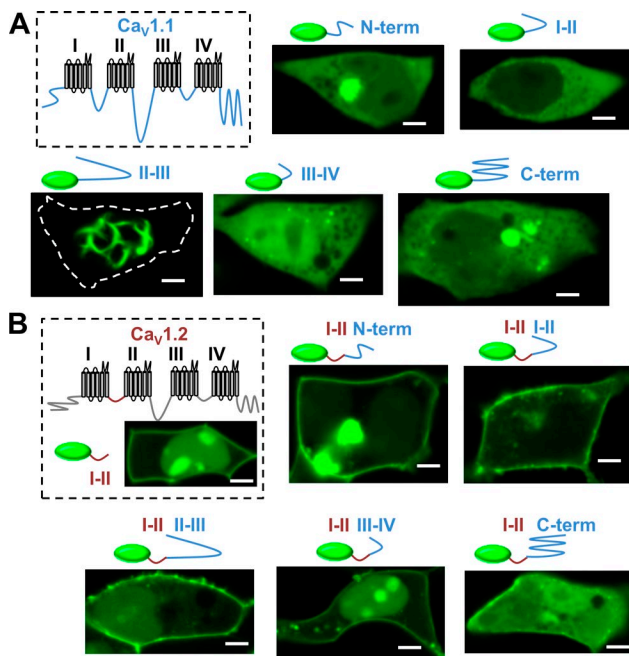


Figure 3. After linking to the I–II loop of Ca_v1.2, the cytoplasmic domains of Ca_v1.1 localize at the surface of tsA201 cells. (A) Representative subcellular distributions in tsA201 cells of GFP-tagged cytoplasmic domains of Ca_v1.1 (schematically represented in the dashed box). For the II–III loop, dashed line indicates cell surface. **(B)** The GFP-tagged I–II loop of Ca_v1.2 (indicated in brown) is concentrated at the cell surface both in isolation (dashed box) and when attached to the cytoplasmic domains of Ca_v1.1 (indicated in blue). Bars, 5 μm.

the three Stac proteins and the Ca_v1.1 II–III loop was also evident in the Pearson’s coefficients for colocalization (Fig. 10 A).

To identify subregions of the Ca_v1.1 II–III loop important for the Stac protein interaction, we focused on Stac3, because it is the only isoform highly expressed in skeletal muscle. In particular, we coexpressed Stac3-RFP with 69-residue fragments of the II–III loop corresponding to the N- or C-terminal halves (rabbit Ca_v1.1 residues 662–730 or 731–799, respectively) or the central region (residues 697–765). These fragments are illustrated schematically in Fig. 5, with orange indicating the residues contained within the critical domain for skeletal-type EC coupling (Nakai et al., 1998; Grabner et al., 1999; Wilkens et al., 2001). Stac3 did not associate with the N-terminal fragment of the loop (Fig. 5 B), but it did associate with the central (Fig. 5 C) and C-terminal fragments (Fig. 5 D and Fig. 10 B). Significantly, the central fragment contained all of the critical domain residues (720–765), and the C-terminal fragment contained most of them (731–765).

As a further test of the importance of the II–III loop critical domain residues, we coexpressed Stac3-RFP in tsA201 cells with polypeptides having the sequence used to replace the II–III loop of Ca_v1.1 in chimeras that had been previously tested for EC coupling by expression in dysgenic myotubes (Grabner et al., 1999; Wilkens et al., 2001). The II–III loop sequence of these chimeras is illustrated in Fig. 6 A together with an indication of whether or not that chimera supported skeletal-type EC coupling. As shown in Fig. 6 (B–E) and Fig. 10 C, Stac3-RFP interacted with the LCS₄₆ and LMS₄₅ loops in tsA201 cells, but not with the LC (cardiac) or LM (*Musca domestica*) loops. In some cells, there appeared to be a

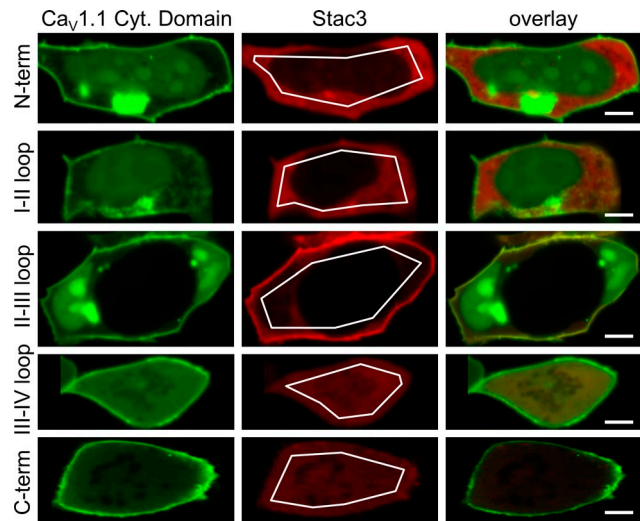


Figure 4. Stac3 associates specifically with the Ca_v1.1 II–III loop in tsA201 cells. Representative images are shown of cells cotransfected with Stac3-RFP and the indicated cytoplasmic domains of Ca_v1.1, which were targeted to the cell surface by being linked to the GFP-tagged I–II loop of Ca_v1.2 (compare Fig. 3). Stac3 associated with the II–III loop of Ca_v1.1, but not with the other cytoplasmic domains. Pearson’s colocalization coefficients are illustrated in Fig. 10 A. Bars, 5 μm.

weak interaction between Stac3-RFP and the LCS₁₈ loop (Fig. 6 F), but this was not apparent in the Pearson’s coefficient (Fig. 10 C).

A pattern of interaction similar to that in tsA201 cells was also observed in dysgenic myotubes cotransfected with Stac3-RFP and GFP-tagged Ca_v1 chimeras in which the II–III loop was replaced by the sequences illustrated in Fig. 6 A. In dysgenic myotubes, GFP-Ca_v1.1 and the GFP-tagged chimeras were all arrayed in discrete foci near the cell surface (Fig. 7, A–F, left), as expected

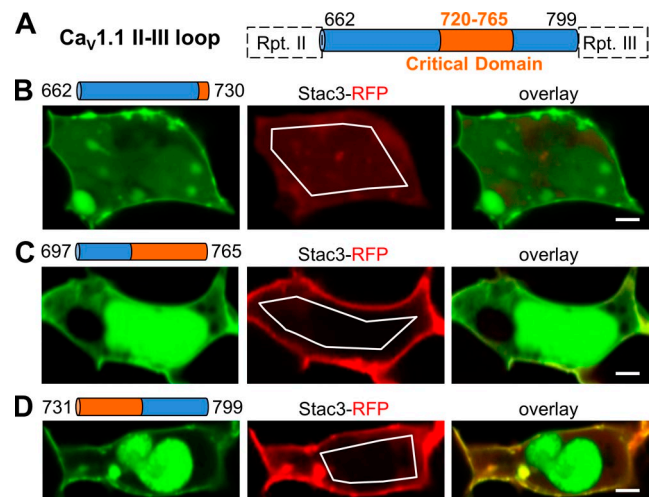


Figure 5. The interaction between Stac3 and the Ca_v1.1 II–III loop depends on residues constituting the critical domain. (A) Schematic representation of the II–III loop of rabbit Ca_v1.1 (residues 662–799), with orange indicating the critical domain (residues 720–765). **(B–D)** Representative images of tsA201 cells cotransfected with Stac3-RFP and the indicated II–III loop fragments linked to the GFP-tagged I–II loop of Ca_v1.2. Stac3 interacted only with segments of the II–III loop containing all (C) or most (D) of the critical domain (see Fig. 10 B for Pearson’s colocalization coefficients). Bars, 5 μm.

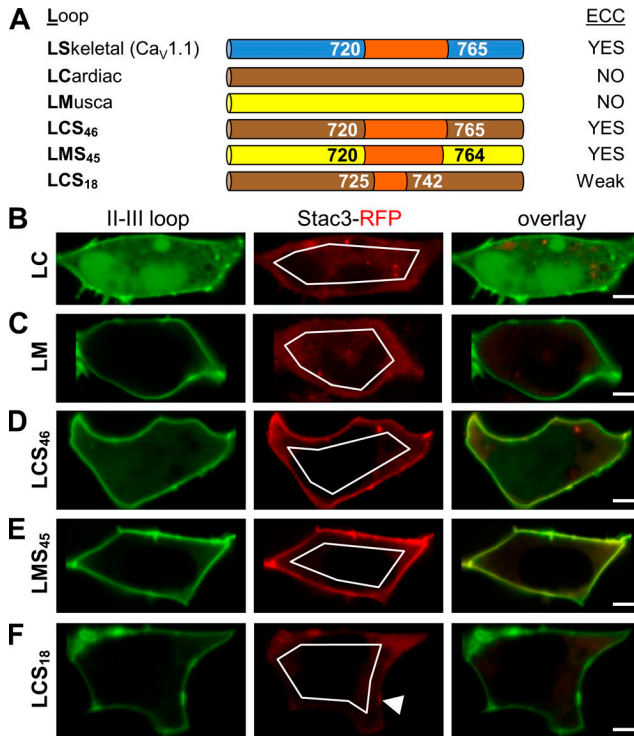


Figure 6. Stac3 interacts in tsA201 cells with chimeric Ca_v II-III loops that contain the critical domain. (A) Summary of II-III loops and their ability, demonstrated in previous work, to mediate skeletal-type EC coupling (ECC) when substituted for the II-III loop of Ca_v1.1. The designations S, C, or M indicate sequence from Ca_v1.1 (skeletal), Ca_v1.2 (cardiac), or Ca_v of housefly muscle (*Musca domestica*), respectively. Numbers refer to the first and last residues of Ca_v1.1 sequence. (B-F) Representative images of tsA201 cells cotransfected with Stac3-RFP (red) and the indicated II-III loop constructs linked to the GFP-tagged I-II loop of Ca_v1.2. Besides the obvious interactions with LCS₄₆ (D) and LMS₄₅ (E), there may have been a weak interaction with LCS₁₈ (F, arrowhead), but this was not consistently observed (see Fig. 10 C). Bars, 5 μm.

for targeting to plasma membrane domains forming junctions with the SR (Flucher et al., 1994). In agreement with previous work (Polster et al., 2015; Campiglio and Flucher, 2017), Stac3-RFP coclustered with GFP-Ca_v1.1 when the two constructs were expressed together in dysgenic myotubes (Fig. 7 A). This contrasts with the diffuse distribution of Stac3-RFP when it is expressed alone in dysgenic myotubes (Polster et al., 2015; Campiglio and Flucher, 2017). A similarly diffuse distribution of Stac3-RFP occurred when it was coexpressed with either SkLC (Fig. 7 B) or SkLM (Fig. 7 C), chimeras which have Ca_v1.1 sequence except for a II-III loop replaced by that of either Ca_v1.2 (SkLC) or that of the calcium channel from housefly muscle (SkLM). However, coclustered red and green puncta were present when Stac3-RFP was coexpressed together with GFP-tagged SkLCS₄₆ (Fig. 7 D) or SkLMS₄₅ (Fig. 7 E), in which the critical domain residues 720-765 or 720-764, respectively, had been inserted into the II-III loops of SkLC or SkLM (compare Fig. 6 A). A small amount of coclustering was sometimes observed in dysgenic myotubes transfected with Stac3-RFP and SkLCS₁₈, in which Ca_v1.1 residues 725-742 were inserted into SkLC (Fig. 7 F), but, as for the isolated LCS₁₈ loop in tsA201 cells, colocalization was not obvious in the Pearson's coefficients (Fig. 10 D). Thus, in both tsA201 cells and dysgenic

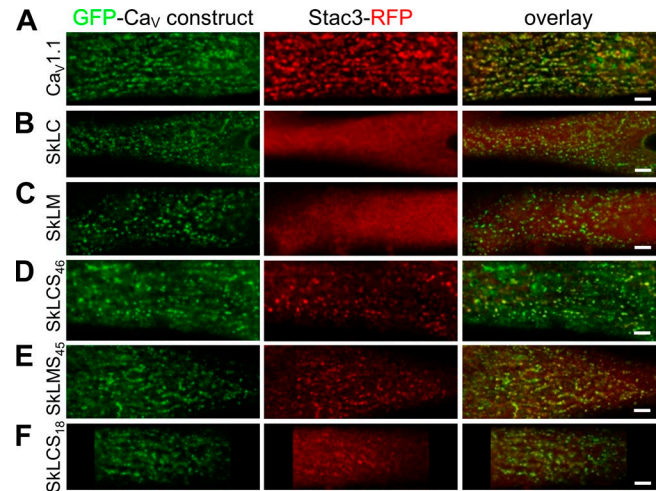


Figure 7. Stac3 interacts in myotubes with full-length Ca_v1.1 chimeras in which the II-III loops contain the critical domain. (A-F) Representative, confocal scans near the surface are shown of dysgenic myotubes cotransfected with Stac3-RFP and GFP-tagged, full-length Ca_v1.1 constructs ("Sk") in which the II-III loop has the sequence indicated to the left of each row of images. Schematic representations of the loop inserts are illustrated in Fig. 6 A, and Pearson's colocalization coefficients are given in Fig. 10 D. Bars, 5 μm.

myotubes, the binding of Stac3 depended on the presence, within the II-III loop, of the sequence critical for EC coupling (Grabner et al., 1999; Wilkens et al., 2001).

Having identified an interaction between the II-III loop critical domain and Stac3, we next investigated regions of Stac3 important for this interaction. Because the data illustrated in Fig. 1 indicated that chimeras between Stac3 and Stac1 or Stac2 were unlikely to be informative, we tested varying sized N-terminal deletions of Stac3 for their ability to interact in tsA201 cells with the center segment of the II-III loop that contains the critical domain (Fig. 8). Stac3 constructs lacking either the first 87 residues (Fig. 8 B), or the first 146 residues (Fig. 8 C), were still able to interact with the critical domain-containing segment of the loop, whereas a construct lacking the 302 N-terminal residues was not (Fig. 8 D). Thus, the first SH3 domain appeared to be required for the binding of Stac3, whereas neither the polyglutamate (pE) nor PKC C1 domains were. As a further test of this latter conclusion, we examined whether the Δ146 Stac3 construct would support functional expression of full-length Ca_v1.1 in tsA201 cells. As shown in Fig. 8 E, Δ146 Stac3 did support expression of Ca_v1.1, although less so than full-length Stac3. The Pearson's colocalization coefficient was also lower for Δ146 Stac3 than for Δ83 Stac3 (Fig. 10 E) or full-length Stac3 (Fig. 10 B). Therefore, the PKC C1 domain appears to have contributed to, but was not required for, the interaction between Stac3 and Ca_v1.1.

Because the function of Ca_v1.1 in EC coupling requires the presence of Stac3 (Polster et al., 2016; Linsley et al., 2017), the question arises as to whether Stac3 is stably associated with Ca_v1.1 complexes. Previous work analyzed the stability of this interaction with recovery of fluorescence after photobleaching of Stac3-GFP associated with Ca_v1.1 in myotubes (Campiglio and Flucher, 2017). At 75 s, the mean recovery, which depends both upon the off rate of bleached Stac3-GFP and the on rate of

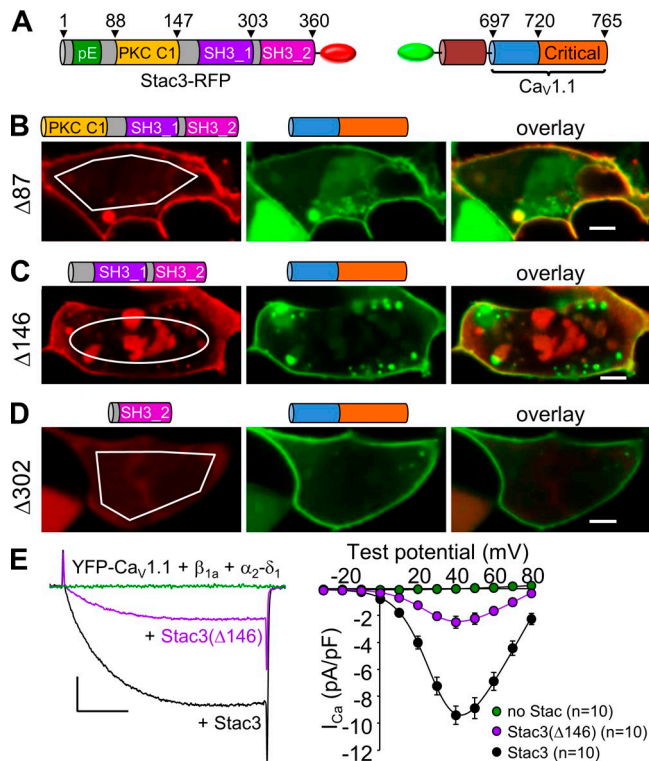


Figure 8. The polyglutamate and PKC C1 domains of Stac3 are not required for its interaction with the critical domain of the Ca_v1.1 II–III loop. (A) Schematic representation (not to scale) and domain architecture of Stac3-RFP and of the GFP-tagged construct containing the middle section of the Ca_v1.1 II–III loop, including the entire critical domain. (B–D) Images of tsA201 cells cotransfected with the indicated Stac3 constructs and the middle section of the II–III loop; for simplicity, the fluorescent and membrane-targeting sequences are not depicted. Stac3 binding occurred for constructs lacking the polyglutamate and PKC C1 domains (B and C), but not for a construct that additionally lacked the first SH3 domain (D). Pearson’s colocalization coefficients for these construct combinations are provided in Fig. 10 E. Bars, 5 μm. (E) Comparison of representative peak Ca²⁺ currents ($V_{rest} = +40$ mV, left) and mean peak I–V relationships (mean ± SEM) in tsA201 cells cotransfected with YFP-Ca_v1.1, β_{1a}, and α₂-δ₁ either without Stac (green) or with Stac3(Δ146) (purple) or Stac3 (black). Calibrations: 3 pA/pF (vertical), 50 ms (horizontal). The Ca²⁺ currents and peak I–V relationships obtained without Stac, or with Stac3, are replotted from Polster et al. (2015).

unbleached Stac3-GFP, was ~25% (Campiglio and Flucher, 2017). Here, we have attempted to characterize the off rate directly and over a longer time period. Specifically, dysgenic myotubes that had been cotransfected with GFP-Ca_v1.1 and Stac3-RFP were permeabilized by a brief exposure to saponin in order to

release unbound Stac3 from the cell. Fig. 9 A illustrates an example of such an experiment with images of a myotube obtained just after (0 min), and at 30 min after, saponin treatment. At 30 min, there was a nearly complete loss of the diffuse red fluorescence, whereas there was much less change in the intensity of the punctate red fluorescence colocalized with GFP-Ca_v1.1. Mean data, given as the ratio of red-to-green punctate fluorescence, are shown in Fig. 9 B and indicate that association between Stac3 and Ca_v1.1 is relatively stable over a time scale of several minutes, with a half-time for dissociation that was on the order of 1 h.

Discussion

Here, we have used fluorescence colocalization and functional measurements to identify amino acid sequences important for the interaction between Stac proteins and Ca_v1.1. In tsA201 cells, we found that all three Stac isoforms colocalized with Ca_v1.1 at the surface (Fig. 1 A), and to a varying extent supported its functional expression as a slowly activating L-type Ca²⁺ channel (Fig. 1 B). In contrast, Ca_v1.1 expressed in tsA201 cells without Stac proteins is retained intracellularly (Polster et al., 2015) and fails to produce Ca²⁺ currents (Fig. 1 B; Polster et al., 2015). Expressed in Stac3-null myotubes, Stac1 and Stac2 were able to restore depolarization-evoked Ca²⁺ transients with peak amplitudes ~40% of those restored by expression of Stac3 (Fig. 2). Thus, all three Stac isoforms appear to interact with Ca_v1.1, supporting its membrane trafficking and its function in EC coupling, with Stac3 clearly being the most effective.

As a tool for identifying Ca_v1.1 cytoplasmic domains important for interacting with the Stac proteins, we took advantage of the observation that these cytoplasmic domains would associate with the surface of tsA201 cells if they were linked to the GFP-tagged I–II loop of Ca_v1.2 (Fig. 3). We found that the II–III loop was the only one of the Ca_v1.1 cytoplasmic domains that was sufficient for binding Stac3 (Fig. 4), Stac1 (Fig. S3), or Stac2 (Fig. S4) in this assay. Also with this approach, we found that Stac3 did not interact with a segment of the II–III loop comprising amino acids 662–730, but it did interact with segments containing either residues 697–765 or 731–799 (Fig. 5). Thus, residues 731–765, which are shared by these latter two segments, likely represent an important binding site for Stac3. Significantly, residues 731–765 constitute the majority of the “critical domain” (amino acids 720–764/5), which was identified on the basis of whether skeletal-type EC coupling could be restored in dysgenic myotubes by the expression of full-length Ca_v1.1 constructs

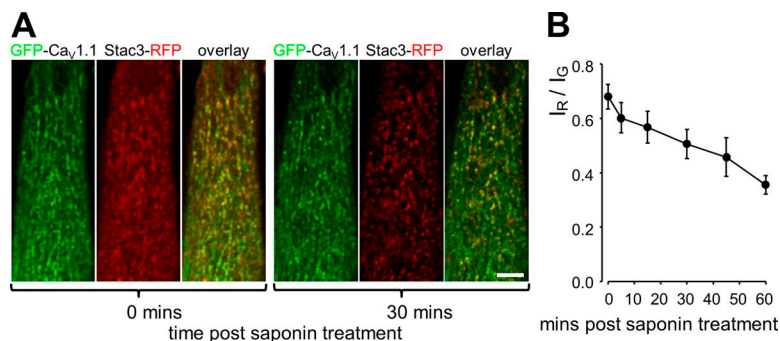


Figure 9. Stac3 is stably associated with Ca_v1.1 in skeletal myotubes. (A) Confocal images, acquired with identical settings, of the surface of a dysgenic myotube cotransfected with GFP-Ca_v1.1 and Stac3-RFP immediately (left) and 30 min (right) after saponin permeabilization to release unbound Stac3. Bar, 5 μm. (B) Mean ratios ± SEM of red to green fluorescence in colocalized puncta as a function of time after saponin treatment ($n = 7$ from two independent culture preparations from dysgenic mice).

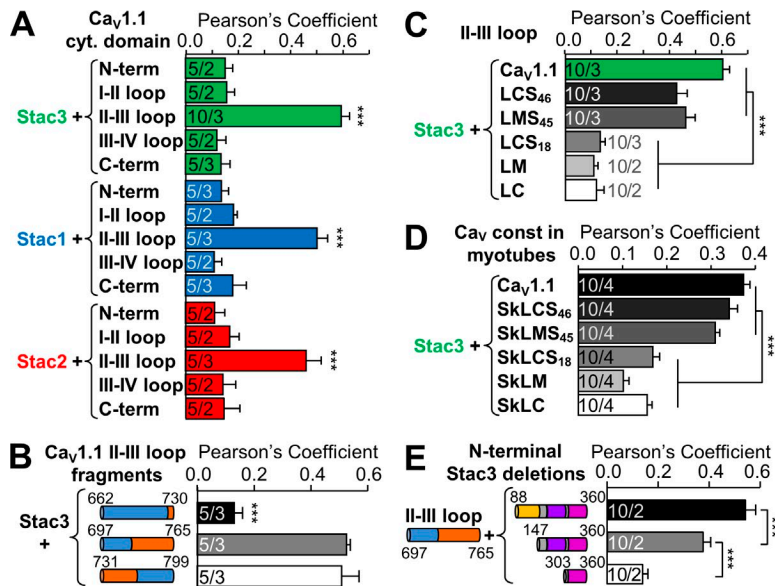


Figure 10. Pearson's coefficients for colocalization of the indicated Ca_v and Stac constructs. (A–E) The constructs were expressed in either tsA201 cells (A–C and E) or dysgenic myotubes (D). The data are presented as mean \pm SEM, and for each combination of constructs, both the number of images analyzed and the number of independent transfections are shown on the plots (first and second number, respectively). Representative images are as follows: A, Stac3 (Fig. 4), Stac1 (Fig. S3), and Stac2 (Fig. S4); B, Fig. 5; C, Fig. 6; D, Fig. 7; and E, Fig. 8 (B–D). ***, $P < 0.001$. Although not indicated on the figure, Stac3 plus either LCS_{46} or LMS_{45} (C) differed from Stac3 plus the $Ca_v1.1$ II–III loop ($P < 0.001$), and Stac3 plus SkLM (panel D) differed from Stac3 plus LCS_{18} ($P < 0.001$) and from Stac3 plus SkLC ($P < 0.008$). Note that the same data for Stac3 plus the $Ca_v1.1$ II–III loop are plotted in both A and C.

containing chimeric II–III loops (Nakai et al., 1998; Grabner et al., 1999; Wilkens et al., 2001). Thus, we additionally tested the interaction of Stac3 both with the chimeric loops expressed in tsA201 cells without the flanking $Ca_v1.1$ sequence (Fig. 6) and with the full-length $Ca_v1.1$ constructs containing the chimeric II–III loops expressed in dysgenic myotubes (Fig. 7). For both the isolated loops and the full-length chimeras, the colocalization with Stac3 correlated (Fig. 10) with the ability of the full-length chimeras to mediate skeletal-type Ca^{2+} release, which was shown to be strong for $SkCLS_{46}$ and $SkLMS_{45}$, absent for $SkLC$ and $SkLM$, and very weak for $SkLCS_{18}$ (Grabner et al., 1999; Wilkens et al., 2001). The rate of release was found to be approximately fivefold lower for $SkLCS_{18}$ than for $SkLCS_{46}$ (Grabner et al., 1999). A similar reduction in the binding affinity for Stac3 could account for the lack of colocalization observed in cells coexpressing Stac3 with LCS_{18} (Fig. 6 F) or $SkLCS_{18}$ (Fig. 7 F). Thus, our results indicate that the ability of chimeric II–III loops to mediate skeletal-type EC coupling requires that they can bind Stac3.

In addition to investigating the determinants of the $Ca_v1.1$ II–III loop that govern its interaction with Stac3, we also performed an analysis of the domains of Stac3 important for this interaction. We found that a Stac3 construct which lacked the polyglutamate and PKC C1 domains still colocalized with a segment of the II–III loop containing residues 731–765 (Fig. 8 C) and was able to support functional expression of full-length $Ca_v1.1$, although to a lesser extent than full-length Stac3 (Fig. 8 E). A Stac3 construct with a larger N-terminal truncation, which additionally deleted the first of the two SH3 domains, did not appear to interact with this segment of the II–III loop (Figs. 8 D and 10 E).

Fig. 11 illustrates the sequence of the $Ca_v1.1$ II–III loop residues 731–765, which our work indicates are likely to contain a high affinity binding site for Stac3. Previous work had shown that an anti- $Ca_v1.1$ monoclonal antibody (Morton and Froehner, 1987) binds to an epitope (amino acids 737–744) that is located within this region (Fig. 11) and is accessible in fixed and permeabilized muscle cells (Kugler et al., 2004a). Thus, amino acids 737–744 can likely be excluded as contributing to the binding of

Stac3. The upstream amino acids (731–736) also seem unlikely to contribute significantly to Stac3 binding, because this binding was too weak to be detected for the chimeras LCS_{18} (Fig. 6 F) or $SkLCS_{18}$ (Fig. 7 F) despite their having $Ca_v1.1$ sequence for residues 725–742. Thus, $Ca_v1.1$ residues 745–765 may represent the likeliest region for high-affinity binding of Stac3, especially because this region contains adjacent PxxP motifs with a shared central proline (Fig. 11, green bar), a sequence motif to which SH3 domains have been shown to bind (Alexandropoulos et al., 1995; Gerhardstein et al., 2000; Zarrinpar et al., 2003). It should be noted that although the binding of Stac3 to $Ca_v1.1$ appears to be necessary for EC coupling, it is clearly not sufficient. For example, skeletal-type EC coupling depends on specific amino acid sequence within the β_{1a} auxiliary subunit of $Ca_v1.1$ (Beurg et al., 1999; Eltit et al., 2014), whereas Stac3 binds to $Ca_v1.1$ even when β_{1a} is entirely absent (Polster et al., 2015). Additionally, the critical domain of the $Ca_v1.1$ II–III loop appears to have an importance beyond that of the binding of Stac3. In particular, mutating the phenylalanine at position 741 to threonine, which is found at the corresponding position of $Ca_v1.2$, causes a $\sim 75\%$ reduction in EC coupling Ca^{2+} release (Kugler et al., 2004b), despite the fact that this residue is in a region unlikely to be directly involved in binding Stac3 (Fig. 11).

While the work we report on here was under review, another paper appeared in which crystallography and

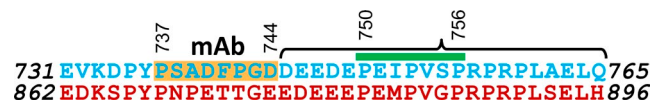


Figure 11. Localization of a potential Stac3 binding site in the primary structure of $Ca_v1.1$. Alignment is shown of the $Ca_v1.1$ II–III loop amino acid residues 731–765 (top) and the corresponding sequence of the $Ca_v1.2$ II–III loop (residues 862–896, bottom). Highlighted in yellow is an epitope (residues 737–744) that binds an anti- $Ca_v1.1$ monoclonal antibody (mAb; Kugler et al., 2004a). The bracket (residues 745–765) represents the likeliest region for Stac3 binding containing adjacent PxxP motifs with a shared central proline (green bar, residues 750–756).

isothermal calorimetry were used to analyze interactions between segments of the Stac proteins and segments of $\text{Ca}_v1.1$ (Wong King Yuen et al., 2017). In their experiments, Wong King Yuen et al. found that binding occurred between $\text{Ca}_v1.1$ residues 728–775 and the region comprising the tandem SH3 domains of all three Stac isoforms, which is consistent with our finding that full-length Stac1, Stac2, and Stac3 all interacted with the $\text{Ca}_v1.1$ II–III loop. Wong King Yuen et al. also found that the first SH3 domain of Stac3 bound to $\text{Ca}_v1.1$ residues 747–760, thus providing direct evidence supporting our hypothesis that the PxxPxxP motif ($\text{Ca}_v1.1$ residues 750–756) represents an important binding determinant for full-length Stac3 (Fig. 11). Perhaps not surprisingly, however, the effects of mutations on the interactions of the small segments of $\text{Ca}_v1.1$ and the Stac proteins that were analyzed by Wong King Yuen et al. appear to be much more profound than those of the same mutations harbored in the full-length proteins. For example, when the mutation W329S, which corresponds to a mutation in Stac3 causing the NAM myopathy (Horststick et al., 2013), was introduced into the isolated, tandem SH3 domains of Stac2, it eliminated binding to $\text{Ca}_v1.1$ loop residues 728–775 (Wong King Yuen et al., 2017). However, full-length Stac3 containing the NAM-causing mutation retains the ability to interact with full-length $\text{Ca}_v1.1$ in both myotubes and tsA201 cells (Polster et al., 2016; Campiglio and Flucher, 2017). In particular, mouse Stac3 containing the NAM mutation and expressed in Stac3 null myotubes resulted in a more than 80% reduction in Ca^{2+} release even though membrane expression of $\text{Ca}_v1.1$ was reduced only ~20% (Polster et al., 2016). As another example, a triple mutation (I752A, P753A, and R757A) within $\text{Ca}_v1.1$ residues 728–775 eliminated the interaction between those residues and the tandem SH3 domains of Stac2 (Wong King Yuen et al., 2017). However, full-length $\text{Ca}_v1.1$ bearing those same three mutations was still able to support EC coupling Ca^{2+} release in dysgenic myotubes, which was ~40% of that for wild-type $\text{Ca}_v1.1$ (Wong King Yuen et al., 2017).

Our conclusions on Stac interactions diverge in two respects from those of another recent study (Campiglio and Flucher, 2017). In particular, using different experimental approaches, they concluded that (1) neither Stac1 nor Stac2 interacts with $\text{Ca}_v1.1$ and (2) the PKC C1 domain is an important determinant of Stac3 binding. In regard to the first of these, they found that neither Stac1 nor Stac2 interacted with coexpressed $\text{Ca}_v1.1$ in dysgenic myotubes. However, we found that both Stac1 and Stac2 interacted with endogenous $\text{Ca}_v1.1$ in Stac3-null myotubes (Fig. 2) and with coexpressed $\text{Ca}_v1.1$ in tsA201 cells (Fig. 1). We think a likely explanation for the different conclusions of the two studies is the absence of endogenous Stac3 in the cells that we studied and its presence in the dysgenic myotubes they studied: this endogenous Stac3 could have occluded the binding of exogenous Stac1 or Stac2. In regard to the second divergent conclusion (the role of the PKC C1 domain), Campiglio and Flucher analyzed, in dysgenic myotubes, the interaction of Stac3/Stac2 chimeras coexpressed with $\text{Ca}_v1.2$ and found that the interaction depended on the presence of the C1 domain of Stac3. We found that in tsA201 cells, a Stac3 construct entirely lacking the PKC C1 domain colocalized with the critical domain of the

coexpressed $\text{Ca}_v1.1$ II–III loop and supported the membrane expression of full-length $\text{Ca}_v1.1$ (Fig. 8). Thus, both the constructs ($\text{Ca}_v1.2$ in their study vs $\text{Ca}_v1.1$ in ours) and the expression systems were different in the two studies. Additionally, we think it is likely that the binding determinants governing the interactions between the Stac proteins and $\text{Ca}_v1.1$ differ from those governing the interactions with $\text{Ca}_v1.2$. For example, Campiglio and Flucher found that in dysgenic myotubes, there was no interaction between Stac1 and $\text{Ca}_v1.1$ but a significant interaction between Stac1 and $\text{Ca}_v1.2$.

Interestingly, a PxxPxxP motif, like that in the $\text{Ca}_v1.1$ II–III loop, is also present in the cardiac ($\text{Ca}_v1.2$) II–III loop (Fig. 11), but we found that Stac3 does not bind to the full-length cardiac II–III loop either as an isolated fragment in tsA201 cells (Fig. 6 B) or when substituted for the II–III loop of $\text{Ca}_v1.1$ in myotubes (Fig. 7). This lack of binding could be a consequence of the amino acid differences between $\text{Ca}_v1.1$ and $\text{Ca}_v1.2$ within, and flanking, the PxxPxxP motif. Alternatively, the full-length cardiac II–III loop might have a secondary structure that prevents such binding. Nonetheless, it is noteworthy that Stac3 did interact with full-length $\text{Ca}_v1.2$ in tsA201 cells and alter its inactivation (Polster et al., 2015). Moreover, Wong King Yuen et al. (2017) showed that a Stac3 construct lacking SH3 domains was still able to slow inactivation of $\text{Ca}_v1.2$ in oocytes. Thus, it appears that neither the II–III loop nor the SH3 domains are involved in the interaction between Stac3 and $\text{Ca}_v1.2$.

One possibility for the role of Stac3 in EC coupling is that it functions as a link between $\text{Ca}_v1.1$ and RyR1. Arguing against this possibility is that Stac3 does not appear to bind to RyR1 in the absence of $\text{Ca}_v1.1$ (Polster et al., 2015). However, it is possible that the interaction with $\text{Ca}_v1.1$ causes Stac3 to assume a conformation that does interact with RyR1. Conversely, one could imagine that the interaction with Stac3 causes $\text{Ca}_v1.1$ and its associated β_{1a} subunit to assume an altered conformation that is necessary for interaction with RyR1. In regard to the latter, it would be of obvious value to have a high resolution structure of $\text{Ca}_v1.1$ assembled with both its auxiliary subunits and Stac3. However, Stac3 appears to have been lost during purification of the $\text{Ca}_v1.1$ complex that is required for structural analysis by cryo-electron microscopy (e.g., Fig. S1 A of Wu et al., 2015). This may have occurred because the interaction between Stac3 and $\text{Ca}_v1.1$ is relatively labile. We found that Stac3 dissociated from $\text{Ca}_v1.1$ clusters with a half-time of ~1 h in permeabilized myotubes at room temperature (Fig. 9). However, two factors may have slowed the dissociation in permeabilized myotubes compared with the dissociation that would occur from detergent-solubilized $\text{Ca}_v1.1$. Specifically, $\text{Ca}_v1.1$ in muscle cells is localized at junctions between the plasma membrane and SR and is present there at a high, localized concentration. Thus, in permeabilized myotubes, diffusion of unbound Stac3 would have been restricted to two dimensions and rebinding of unbound Stac3 could have occurred to nearby $\text{Ca}_v1.1$ moieties (that had already lost Stac3). Accordingly, the dissociation of Stac3 from detergent-solubilized $\text{Ca}_v1.1$ may well be more rapid than we observed for myotubes. Whether or not this is correct, it would seem an important goal for future structural studies to monitor the rate of loss of Stac3 and seek conditions to prevent it.

Acknowledgments

We thank O. Moua for expert technical assistance.

This work was supported by the National Institutes of Health (grants AR055104 and AR052354 to K.G. Beam) and the Muscular Dystrophy Association (grant 479598 to A. Polster). Work in the laboratory of E.N. Olson was supported by the National Institutes of Health (grants HL-077439, HL-111665, HL-093039, DK-099653, and U01-HL-100401) and the Robert A. Welch Foundation (grant 1-0025). B.R. Nelson was supported by a National Institutes of Health predoctoral fellowship.

The authors declare no competing financial interests.

Author contributions: A. Polster and K.G. Beam designed research, performed research, analyzed the data, and wrote the manuscript. B.R. Nelson, S. Papadopoulos, and E.N. Olson contributed new reagents/analytic tools. All authors discussed the results and approved the final version of the manuscript.

Eduardo Ríos served as editor.

Submitted: 2 October 2017

Revised: 5 January 2018

Accepted: 17 January 2018

References

- Adams, B.A., T. Tanabe, A. Mikami, S. Numa, and K.G. Beam. 1990. Intramembrane charge movement restored in dysgenic skeletal muscle by injection of dihydropyridine receptor cDNAs. *Nature*. 346:569–572. <https://doi.org/10.1038/346569a0>
- Alexandropoulos, K., G. Cheng, and D. Baltimore. 1995. Proline-rich sequences that bind to Src homology 3 domains with individual specificities. *Proc. Natl. Acad. Sci. USA*. 92:3110–3114. <https://doi.org/10.1073/pnas.92.8.3110>
- Armstrong, C.M., F.M. Bezanilla, and P. Horowicz. 1972. Twitches in the presence of ethylene glycol bis(β -aminoethyl ether)-N,N'-tetracetic acid. *Biochim. Biophys. Acta*. 267:605–608. [https://doi.org/10.1016/0005-2728\(72\)90194-6](https://doi.org/10.1016/0005-2728(72)90194-6)
- Avila, G., J.J. O'Brien, and R.T. Dirksen. 2001. Excitation-contraction uncoupling by a human central core disease mutation in the ryanodine receptor. *Proc. Natl. Acad. Sci. USA*. 98:4215–4220. <https://doi.org/10.1073/pnas.071048198>
- Beam, K.G., and C. Franzini-Armstrong. 1997. Functional and structural approaches to the study of excitation-contraction coupling. *Methods Cell Biol.* 52:283–306. [https://doi.org/10.1016/S0091-679X\(08\)60384-2](https://doi.org/10.1016/S0091-679X(08)60384-2)
- Beurg, M., C.A. Ahern, P. Vallejo, M.W. Conklin, P.A. Powers, R.G. Gregg, and R. Coronado. 1999. Involvement of the carboxy-terminus region of the dihydropyridine receptor β 1a subunit in excitation-contraction coupling of skeletal muscle. *Biophys. J.* 77:2953–2967. [https://doi.org/10.1016/S0006-3495\(99\)77128-6](https://doi.org/10.1016/S0006-3495(99)77128-6)
- Campiglio, M., and B.E. Flucher. 2017. STAC3 stably interacts through its C1 domain with $\text{Ca}_v1.1$ in skeletal muscle triads. *Sci. Rep.* 7:41003. <https://doi.org/10.1038/srep41003>
- Eltit, J.M., C. Franzini-Armstrong, and C.F. Perez. 2014. Amino acid residues 489–503 of dihydropyridine receptor (DHPR) β 1a subunit are critical for structural communication between the skeletal muscle DHPR complex and type I ryanodine receptor. *J. Biol. Chem.* 289:36116–36124. <https://doi.org/10.1074/jbc.M114.615526>
- Flucher, B.E., S.B. Andrews, and M.P. Daniels. 1994. Molecular organization of transverse tubule/sarcoplasmic reticulum junctions during development of excitation-contraction coupling in skeletal muscle. *Mol. Biol. Cell.* 5:1105–1118. <https://doi.org/10.1091/mbc.5.10.1105>
- Gerhardstein, B.L., T. Gao, M. Bünemann, T.S. Puri, A. Adair, H. Ma, and M.M. Hosey. 2000. Proteolytic processing of the C terminus of the α_{1c} subunit of L-type calcium channels and the role of a proline-rich domain in membrane tethering of proteolytic fragments. *J. Biol. Chem.* 275:8556–8563. <https://doi.org/10.1074/jbc.275.12.8556>
- Grabner, M., R.T. Dirksen, and K.G. Beam. 1998. Tagging with green fluorescent protein reveals a distinct subcellular distribution of L-type and non-L-type Ca^{2+} channels expressed in dysgenic myotubes. *Proc. Natl. Acad. Sci. USA*. 95:1903–1908. <https://doi.org/10.1073/pnas.95.4.1903>
- Grabner, M., R.T. Dirksen, N. Suda, and K.G. Beam. 1999. The II-III loop of the skeletal muscle dihydropyridine receptor is responsible for the Bi-directional coupling with the ryanodine receptor. *J. Biol. Chem.* 274:21913–21919. <https://doi.org/10.1074/jbc.274.31.21913>
- Horstick, E.J., J.W. Linsley, J.J. Dowling, M.A. Hauser, K.K. McDonald, A. Ashley-Koch, L. Saint-Amant, A. Satish, W.W. Cui, W. Zhou, et al. 2013. Stac3 is a component of the excitation-contraction coupling machinery and mutated in Native American myopathy. *Nat. Commun.* 4:1952. <https://doi.org/10.1038/ncomms2952>
- Kaur, G., A. Pinggera, N.J. Ortner, A. Lieb, M.J. Sinnegger-Brauns, V. Yarov-Yarovoy, G.J. Obermair, B.E. Flucher, and J. Striessnig. 2015. A polybasic plasma membrane binding motif in the I-II linker stabilizes voltage-gated $\text{Ca}_v1.2$ calcium channel function. *J. Biol. Chem.* 290:21086–21100. <https://doi.org/10.1074/jbc.M115.645671>
- Kugler, G., M. Grabner, J. Platzer, J. Striessnig, and B.E. Flucher. 2004a. The monoclonal antibody mAB 1A binds to the excitation-contraction coupling domain in the II-III loop of the skeletal muscle calcium channel α 1S subunit. *Arch. Biochem. Biophys.* 427:91–100. <https://doi.org/10.1016/j.abb.2004.04.007>
- Kugler, G., R.G. Weiss, B.E. Flucher, and M. Grabner. 2004b. Structural requirements of the dihydropyridine receptor α 1S II-III loop for skeletal-type excitation-contraction coupling. *J. Biol. Chem.* 279:4721–4728. <https://doi.org/10.1074/jbc.M307538200>
- Linsley, J.W., I.U. Hsu, W. Wang, and J.Y. Kuwada. 2017. Transport of the α subunit of the voltage gated L-type calcium channel through the sarcoplasmic reticulum occurs prior to localization to triads and requires the β subunit but not Stac3 in skeletal muscles. *Traffic*. 18:622–632. <https://doi.org/10.1111/tra.12502>
- Morton, M.E., and S.C. Froehner. 1987. Monoclonal antibody identifies a 200-kDa subunit of the calcium channel. *J. Biol. Chem.* 262:11904–11907.
- Nakai, J., R.T. Dirksen, H.T. Nguyen, I.N. Pessah, K.G. Beam, and P.D. Allen. 1996. Enhanced dihydropyridine receptor channel activity in the presence of ryanodine receptor. *Nature*. 380:72–75. <https://doi.org/10.1038/380072a0>
- Nakai, J., T. Tanabe, T. Konno, B. Adams, and K.G. Beam. 1998. Localization in the II-III loop of the dihydropyridine receptor of a sequence critical for excitation-contraction coupling. *J. Biol. Chem.* 273:24983–24986. <https://doi.org/10.1074/jbc.273.39.24983>
- Nelson, B.R., F. Wu, Y. Liu, D.M. Anderson, J. McAnally, W. Lin, S.C. Cannon, R. Bassel-Duby, and E.N. Olson. 2013. Skeletal muscle-specific T-tubule protein STAC3 mediates voltage-induced Ca^{2+} release and contractility. *Proc. Natl. Acad. Sci. USA*. 110:11881–11886. <https://doi.org/10.1073/pnas.1310571110>
- Papadopoulos, S., V. Leuranguer, R.A. Bannister, and K.G. Beam. 2004. Mapping sites of potential proximity between the dihydropyridine receptor and RyR1 in muscle using a cyan fluorescent protein-yellow fluorescent protein tandem as a fluorescence resonance energy transfer probe. *J. Biol. Chem.* 279:44046–44056. <https://doi.org/10.1074/jbc.M405317200>
- Polster, A., S. Perni, H. Bichraoui, and K.G. Beam. 2015. Stac adaptor proteins regulate trafficking and function of muscle and neuronal L-type Ca^{2+} channels. *Proc. Natl. Acad. Sci. USA*. 112:602–606. <https://doi.org/10.1073/pnas.1423113112>
- Polster, A., B.R. Nelson, E.N. Olson, and K.G. Beam. 2016. Stac3 has a direct role in skeletal muscle-type excitation-contraction coupling that is disrupted by a myopathy-causing mutation. *Proc. Natl. Acad. Sci. USA*. 113:10986–10991. <https://doi.org/10.1073/pnas.1612441113>
- Schredelseker, J., A. Dayal, T. Schwerte, C. Franzini-Armstrong, and M. Grabner. 2009. Proper restoration of excitation-contraction coupling in the dihydropyridine receptor β 1a-null zebrafish relaxed is an exclusive function of the β 1a subunit. *J. Biol. Chem.* 284:1242–1251. <https://doi.org/10.1074/jbc.M807767200>
- Takahashi, S.X., J. Miriyala, L.H. Tay, D.T. Yue, and H.M. Colecraft. 2005. A $\text{Ca}_v\beta$ SH3/guanylate kinase domain interaction regulates multiple properties of voltage-gated Ca^{2+} channels. *J. Gen. Physiol.* 126:365–377. <https://doi.org/10.1085/jgp.200509354>
- Tanabe, T., K.G. Beam, J.A. Powell, and S. Numa. 1988. Restoration of excitation-contraction coupling and slow calcium current in dysgenic muscle by dihydropyridine receptor complementary DNA. *Nature*. 336:134–139. <https://doi.org/10.1038/336134a0>
- Wilkens, C.M., N. Kasielke, B.E. Flucher, K.G. Beam, and M. Grabner. 2001. Excitation-contraction coupling is unaffected by drastic alteration of the sequence surrounding residues L720-L764 of the α 1S II-III

- loop. *Proc. Natl. Acad. Sci. USA.* 98:5892–5897. <https://doi.org/10.1073/pnas.101618098>
- Wong King Yuen, S.M., M. Campiglio, C.C. Tung, B.E. Flucher, and F. Van Petegem. 2017. Structural insights into binding of STAC proteins to voltage-gated calcium channels. *Proc. Natl. Acad. Sci. USA.* 114:E9520–E9528. <https://doi.org/10.1073/pnas.1708852114>
- Wu, J., Z. Yan, Z. Li, C. Yan, S. Lu, M. Dong, and N. Yan. 2015. Structure of the voltage-gated calcium channel Cav1.1 complex. *Science.* 350:aad2395. <https://doi.org/10.1126/science.aad2395>
- Zarrinpar, A., R.P. Bhattacharyya, and W.A. Lim. 2003. The structure and function of proline recognition domains. *Sci. STKE.* 2003:RE8.